Biodistribution and Dosimetry of ^{18}F-Meta-Fluorobenzylguanidine: A First-in-Human PET/CT Imaging Study of Patients with Neuroendocrine Malignancies

Neeta Pandit-Taskar[1,2], Pat Zanzonico[3], Kevin D. Staton[4], Jorge A. Carrasquillo[1,2], Diane Reidy-Lagunes[5], Serge Lyashchenko[4,6], Eva Burnazi[4,5], Hanwen Zhang[4], Jason S. Lewis[4,6], Ronald Blasberg[6,7], Steven M. Larson[1,2,6], Wolfgang A. Weber[1], and Shakeel Modak[8]

[1]Molecular Imaging and Therapy Service, Department of Radiology, Memorial Sloan Kettering Cancer Center, New York, New York; [2]Department of Radiology, Weill Cornell Medical College, New York, New York; [3]Department of Medical Physics, Memorial Sloan Kettering Cancer Center, New York, New York; [4]Radiochemistry & Molecular Imaging Probe Core Facility, Memorial Sloan Kettering Cancer Center, New York, New York; [5]GI Oncology Service, Department of Medicine, Memorial Sloan Kettering Cancer Center, New York, New York; [6]Molecular Pharmacology Program, Memorial Sloan Kettering Cancer Center, New York, New York; [7]Department of Neurology, Memorial Sloan Kettering Cancer Center, New York, New York; and [8]Pediatric Oncology Service, Department of Medicine, Memorial Sloan Kettering Cancer Center, New York, New York

^{123}I-meta-iodobenzylguanidine (^{123}I-MIBG) imaging is currently a mainstay in the evaluation of many neuroendocrine tumors, especially neuroblastoma. ^{123}I-MIBG imaging has several limitations that can be overcome by the use of a PET agent. ^{18}F-meta-fluorobenzylguanidine (^{18}F-MFBG) is a PET analog of MIBG that may allow for single-day, high-resolution quantitative imaging. We conducted a first-in-human study of ^{18}F-MFBG PET imaging to evaluate the safety, feasibility, pharmacokinetics, and dosimetry of ^{18}F-MFBG in neuroendocrine tumors (NETs). **Methods:** Ten patients (5 with neuroblastoma and 5 with paraganglioma/pheochromocytoma) received 148–444 MBq (4–12mCi) of ^{18}F-MFBG intravenously followed by serial whole-body imaging at 0.5–1, 1–2, and 3–4 after injection. Serial blood samples (a total of 6) were also obtained starting at 5 min after injection to as late as 4 h after injection; whole-body distribution and blood clearance data, lesion uptake, and normal-tissue uptake were determined, and radiation-absorbed doses to normal organs were calculated using OLINDA. **Results:** No side effects were seen in any patient after ^{18}F-MFBG injection. Tracer distribution showed prominent activity in the blood pool, liver, and salivary glands that decreased with time. Mild uptake was seen in the kidneys and spleen, which also decreased with time. Urinary excretion was prominent, with an average of 45% of the administered activity in the bladder by 1 h after injection; whole-body clearance was monoexponential, with a mean biologic half-life of 1.95 h, whereas blood clearance was biexponential, with a mean biologic half-life of 0.3 h (58%) for the rapid α phase and 6.1 h (42%) for the slower β phase. The urinary bladder received the highest radiation dose with a mean absorbed dose of 0.186 $\pm$ 0.195 mGy/MBq. The mean total-body dose was 0.011 $\pm$ 0.011 mGy/MBq, and the effective dose was 0.023 $\pm$ 0.012 mSv/MBq. Both skeletal and soft-tissue lesions were visualized with high contrast. The SUVmax (mean $\pm$ SD) of lesions at 1–2 h after injection was 8.6 $\pm$ 9.6. **Conclusion:** Preliminary data show that ^{18}F-MFBG imaging is safe and has favorable biodistribution and kinetics with good targeting of lesions. PET imaging with ^{18}F-MFBG allows for same-day imaging of NETs. ^{18}F-MFBG appears highly promising for imaging of patients with NETs, especially children with neuroblastoma.

Key Words: ^{18}F-MFBG; neuroendocrine; neuroblastoma; dosimetry; MIBG

J Nucl Med 2018; 59:147–153
DOI: 10.2967/jnumed.117.193169

Imaging plays a critical role in the diagnosis, staging, and follow-up of neuroendocrine tumors (NETs). Currently, ^{131}I-meta-iodobenzylguanidine (^{131}I-MIBG) and ^{123}I-MIBG are widely used in NETs overexpressing the norepinephrine transporter, and ^{123}I-MIBG is routinely used for staging and follow-up of patients with neuroblastoma (*1–8*). ^{123}I-MIBG imaging is also used for the evaluation of disease extent and suitability for ^{131}I-MIBG therapy.

However, ^{123}I-MIBG imaging has significant limitations, including a 2-d imaging schedule, with injection on the first day and imaging 24 h later (*3*); and a need for thyroid protection with supersaturated potassium iodide before ^{123}I-MIBG injection. Further, compared with PET, the images have poorer resolution and limited quantitative accuracy, which is typically associated with γ-camera imaging. These differences compromise sensitivity and the ability to evaluate tumor burden and tumor accumulation. Therefore, there is a clinical need for a PET imaging agent that would allow for same-day imaging with superior resolution and quantitation of the tracer uptake in lesions associated with PET imaging.

The PET imaging tracer ^{124}I-MIBG has been studied previously (*9*), but the complex decay scheme, including the emission of high-energy cascade γ-rays, leads to poorer image quality, less reliable quantification, and unfavorable dosimetry (*10*). Furthermore, ^{124}I is not widely available for clinical use. ^{18}F-fluorodopamine, a dopamine analog, and ^{18}F-fluorodopa PET have also been used to image noradrenaline and amino acid transporter expression, respectively, in neuroendocrine malignancies; however, the experience is limited, particularly in patients with neuroblastoma (*11,12*).

Received Mar. 10, 2017; revision accepted Jun. 8, 2017.
For correspondence or reprints contact: Neeta Pandit-Taskar, Molecular Imaging and Therapy Service, Department of Radiology, Memorial Sloan Kettering Cancer Center, 1275 York Ave., Box 77, New York, NY 10065.
E-mail: pandit-n@mskcc.org
Published online Jul. 13, 2017.
COPYRIGHT © 2018 by the Society of Nuclear Medicine and Molecular Imaging.

^{11}C-hydroxyephedrine, a catecholamine analog (*13*), has also been shown to target tumors of the sympathetic nervous system. Current clinical data are again limited, and use of a short-lived isotope limits its use. These tracers are also currently limited in availability. There is a need for a NET imaging agent that allows for single-day imaging and that will enable faster evaluation of disease sites with high sensitivity within a more convenient imaging schedule. Given our extensive clinical experience with ^{123}I-MIBG, a PET tracer such as an ^{18}F-labeled analog of MIBG is appealing.

^{18}F-labeled meta-fluorobenzylguanidine (^{18}F-MFBG) was synthesized to overcome these limitations, and preclinical studies have shown a similarity to ^{123}I-MIBG (*14*). In xenografts, ^{18}F-MFBG showed a similar lesion uptake, with significantly faster blood clearance than ^{123}I-MIBG, enabling high-contrast visualization of lesions as early as 1 h after injection (*15*).

On the basis of these preclinical data, we initiated a first-in-human study (NCT 02348749) to evaluate the safety, pharmacokinetics, and radiation dosimetry of ^{18}F-MFBG in patients with neuroblastoma and pheochromocytoma/paragangliomas. We report the results of the safety, biodistribution, pharmacokinetics, and organ dosimetry of ^{18}F-MFBG in these patients.

MATERIALS AND METHODS

A prospective study of PET imaging with ^{18}F-MFBG was performed. ^{18}F-MFBG was administered under an Investigational New Drug application (IND# 125108) approved by the Food and Drug Administration. The protocol was approved by the Institutional Review Board, and all patients or their legal guardians provided written informed consent.

Patients

Patients with confirmed neuroblastoma or paraganglioma/pheochromocytoma with evidence of evaluable disease or lesions on ^{123}I-MIBG imaging were eligible. Additional eligibility criteria included a performance status of 60 or higher on the Karnofsky or Lansky scale and adequate hepatic and renal function defined as no toxicity greater than grade 2 (CTC 4.0).

^{18}F-MFBG Preparation

^{18}F-MFBG was manufactured at the Memorial Sloan Kettering Radiochemistry and Molecular Imaging Probes Core Facility in compliance with the requirements specified in the Chemistry, Manufacturing, and Controls section of a Food and Drug Administration–approved IND. Clinical ^{18}F-MFBG batches for the first 4 patients were prepared using the original manual method described previously (*16*). Subsequently, the method was changed to a less complex synthesis, using the diaryliodonium salt (ALP)-MFBG precursor, supplied by Ground Fluor Pharmaceuticals, Inc. The revised synthesis, derived from the methods published by Hu et al. (*17*), involved nucleophilic incorporation of ^{18}F-fluoride into the ^{18}F-MFBG precursor, ALP-MFBG (7.5 mg dissolved in 1 mL of acetonitrile), at 120°C for 20 min, followed by removal of protective groups by acid hydrolysis, reversed-phase preparatory high-performance liquid chromatography (HPLC) purification, and terminal sterilization using a 0.22-μm sterilizing filter. The final ^{18}F-MFBG drug product was formulated in 15 mL of ammonium acetate buffer and sterile water for injection (United States Pharmacopeia).

The final ^{18}F-MFBG drug product batches underwent quality control testing, before batch release for patient administration. Radiochemical purity was more than 90%, as determined by reversed-phase HPLC; radiochemical identity was confirmed by comparison to a reference standard response on the HPLC; endotoxin content was less than 5 EU/mL, as measured by the portable test system supplied by Charles River Laboratories; sterilizing filter integrity pressure was more than 50 ψ, as measured by the bubble point method; pH was 3.5–8.0, as measured by pH strips; residual acetonitrile concentration was less than 270 μg/mL, as measured by gas chromatography; appearance was a clear and particle-free solution, as determined by a visual inspection check; and radionuclide identity was verified, as measured by radioactive half-life determination. Sterility testing, using the direct medium inoculation method, was performed after release. Specific activity (MBq/μg) determinations were performed on the initial ^{18}F-MFBG validation batches and calibrated to the end of synthesis time; these were calculated by dividing the total measured radioactivity at the end of synthesis time by the total mass of ^{18}F-MFBG present in the final product, as measured by HPLC.

^{18}F-MFBG Administration

A dose of 148–444 MBq (4–12 mCi) of ^{18}F-MFBG was administered as a slow intravenous bolus over 1 min, followed by a saline flush. Patients were not required to fast. No premedications were administered, and no patients were taking any medications known to interfere with MIBG uptake (*3*). Patients were monitored for at least 3 h after injection with vitals and for any reactions or adverse events and later at 24 h follow-up. Side effects and reactions were graded according to Common Terminology Criteria for Adverse Events, version 4.0.

^{18}F-MFBG Scans

Scanning included dynamic imaging for the first 30 min with images acquired in list mode, 128 × 128 matrix (6 frames for 5 s each, followed by 3 frames for 10 s each, 4 frames for 1 min each, 2 frames for 2.5 min each, 2 frames for 5 min each, and 1 frame for 10 min) over the chest (including cardiac blood pool, lung, and liver) followed by whole-body (vertex to feet) imaging within the first hour after injection, a second whole-body scan at 1–2 h, and a third whole-body scan at 3–4 h after injection. A single low-dose CT scan, at 80 mA for adults and a weight-based scaled mA for children, was obtained. The 2 remaining PET/CT scans were acquired with an ultra-low-dose CT at 10 mA for attenuation. All scans were obtained on the same scanner (Discovery 710; 3-dimensional) in 3-dimensional mode with a 3-min acquisition time per field of view for the torso (vertex to pelvis) and 1- to 2-min field of view for the lower limbs. Images were reconstructed using a manufacturer-provided iterative reconstruction algorithm and attenuation and scatter corrections similar to ^{18}F-FDG imaging.

Blood Clearance Measurements

Multiple venous blood samples were obtained, including a baseline sample before injection of ^{18}F-MFBG, at 5 ± 2, 15 ± 5, 30 ± 5, 60 ± 5, 90 ± 10, 120 ± 10, and 180 ± 10 min after injection. Activity in blood (aliquots of about 500 μL) was measured in duplicate using a NaI (Tl) γ-counter (Wallac Wizard 1480 automatic γ-counter; Perkin Elmer) together with appropriate standards. The measured activity concentrations were converted to percentage injected activity per liter. Metabolite analysis of activity in plasma was performed by reversed-phase HPLC with in-line radiation detection on samples obtained up to at least 120 min after injection in all patients.

Whole-Body and Blood Parameters

Activity in the whole body was determined on the basis of whole-body scans; the first scan was obtained before voiding. A monoexponential function was fitted to the whole-body activity data and a biexponential function to the blood activity concentration data (*18*). Values of cumulated activity per unit administered activity (residence time) for whole body (in h) and blood (in h/L), τ, were calculated according to the formula $\tau = \tilde{A}/A_0$ where $\tilde{A}$, the cumulated activity, was estimated by integration of the time–activity curve and A_0 was the administered activity. Effective and biologic clearance rates and corresponding half-times were derived from the fitted curves.

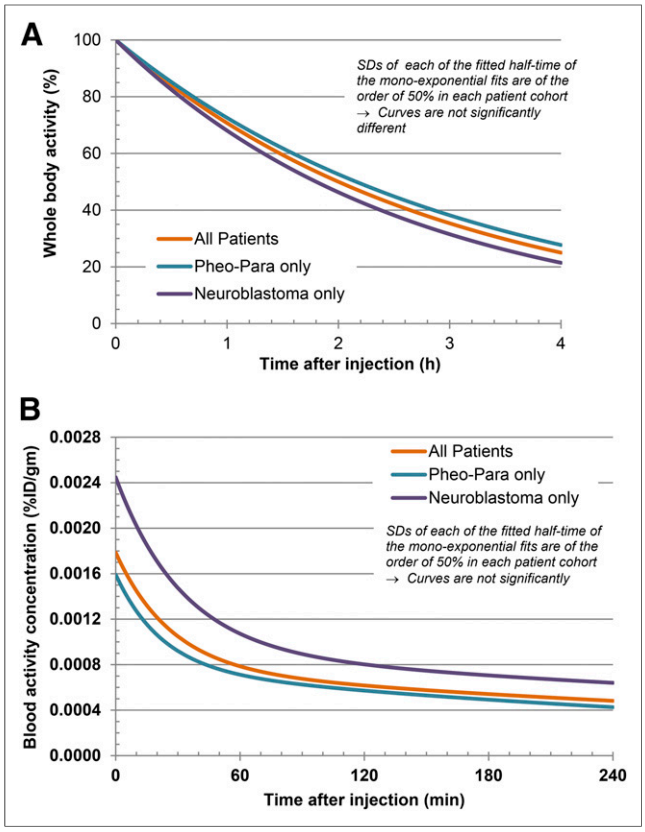

FIGURE 1. Whole-body (A) and -blood (B) clearance time–activity curves. Whole-body activity showed monoexponential clearance, and blood activity showed biexponential clearance. Para = paraganglioma; Pheo = pheochromocytoma.

Normal-Organ Uptake and Dosimetry

Regions of interest were drawn on the PET images over normal organs, including lacrimal gland, salivary gland, thyroid gland, lung, right atrium, ventricular myocardium, liver, renal parenchyma, pancreas, spleen, adrenal gland, and bladder. Multiple regions of interest were used to generate volumes of interest of a representative site in organs that were copied to all scans (Hermes Medical Solutions). Activity concentration per unit mass (kBq/g) was generated for organs, and area under the activity concentration–time curves were integrated. Whole-organ areas under the curve were estimated by multiplying the activity concentration area under the curve by the respective organ masses, as given in the OLINDA/EXM dosimetry program, which was then used to derive the organ residence times (*19*).

Absorbed radiation doses to the whole body and various organs and the effective dose were calculated using the image-derived cumulated activities/residence time and the OLINDA/EXM program (*19*). The anatomic model in OLINDA for which whole-body mass most closely matched that of the patient was used, with the organ masses in OLINDA then scaled in proportion to the patient-to-anatomic model whole-body mass ratio.

RESULTS

Patients and ^{18}F-MFBG Administration

Ten patients, including 5 with neuroblastoma (age, 5–23; 3 males and 2 females) and 5 with paraganglioma/pheochromocytoma (age 16–68; 2 males and 3 females), were imaged. All patients with neuroblastoma had recurrent disease. The patients with paraganglioma/pheochromocytoma had measurable and progressive disease as noted on standard imaging (CT/MRI/MIBG scanning), performed as standard of care. All patients had prior ^{123}I-MIBG scans obtained within 4 wk before the ^{18}F-MFBG PET scan that included whole-body planar imaging and SPECT/CT of the chest, abdomen, and pelvis. The injections were tolerated well, with no reactions or adverse events seen in any patients. The injected activity ranged from 162 to 436 MBq (4.37–11.8 mCi). The mean specific activity was 610.5 MBq/μg (16.5 mCi/μg) (range, 573.5 - > 1,061.9 MBq/μg or 15.5 - > 28.7 mCi/μg) for ^{18}F-MFBG, produced via the initial radiosynthesis method, and 138.1 MBq/μg (3.73 mCi/μg) (range, 16.7–442.2 MBq/μg or 0.45–11.95 mCi/μg) for the ALP-MFBG–based radiosynthesis method. Radiochemical purity was greater than 95% in all batches.

Metabolite analysis showed that MFBG (mean ± SD), eluted with a retention time of 12.5 min, accounted for 90.0% ± 6.7% and 92.4 ± 4.6 of the plasma-borne activity in the blood samples obtained at 60 and 120 min after injection, respectively. The ^{18}F-MFBG thus indicated excellent stability in vivo.

Whole-Body and Blood Kinetics

Blood clearance was biexponential, characterized by an initial rapid phase followed by a mean (±SD) half-time of biologic clearance of 0.31 ± 0.20 h (range, 0.12–0.35 h) for the fast component, α phase (57.6%), and 6.09 ± 3.8 h (range, 2.2–15.0 h) for the slow component, β phase (42.4%) (Fig. 1A). For patients with paraganglioma/pheochromocytoma, the mean (±SD) half-time of clearance was 0.26 ± 0.12 h for the α phase (57.3%) and 4.8 h ± 2.7 h (42.7%) for the β phase, whereas corresponding values for

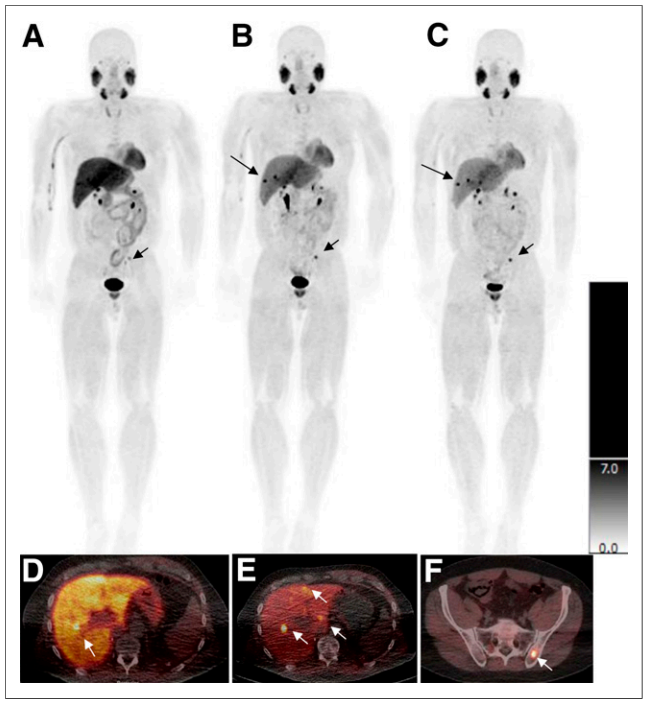

FIGURE 2. Patient with metastatic pheochromocytoma. Whole-body maximum-intensity-projection scans of ^{18}F-MFBG obtained 30–60 min after injection (A), 1–2 h after injection (B), and 3–4 h after injection (C) as against a uniform SUV scale (right bar). Lesions are distinctly seen in the liver at 1–2 h and 3–4 h after injection (B and C; arrows). Fused images show lesions more distinctly in liver (D and E; arrows). Lesion in maximum-intensity-projection image is localized to left iliac bone (F; short arrow).

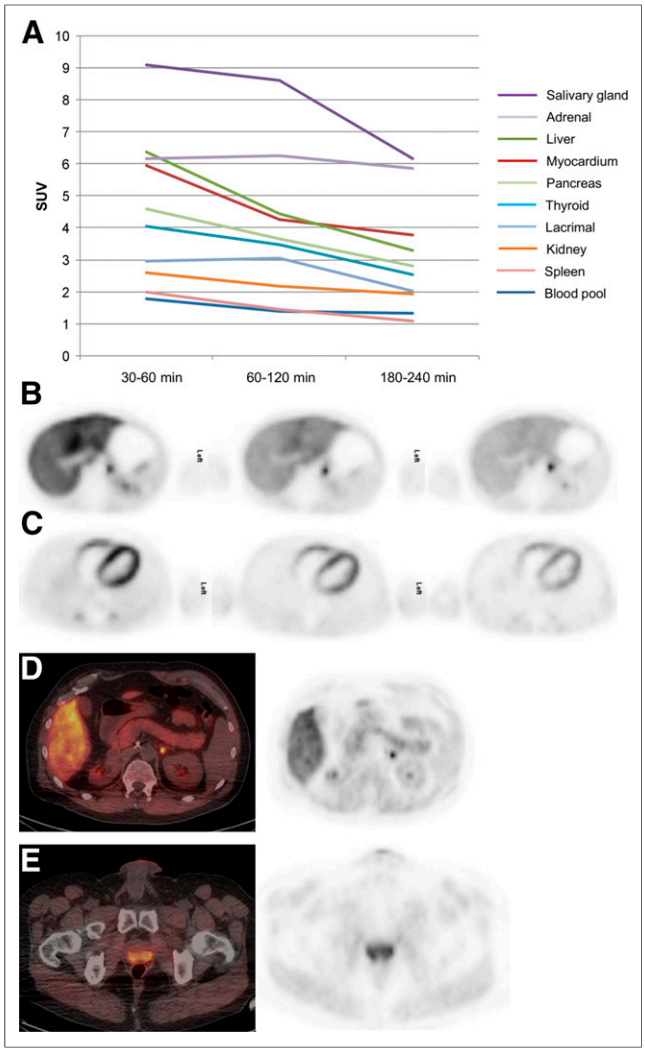

FIGURE 3. Uptake in normal organs at various scan times after injection. (A) Uptake decreases from scan 1 (0.5–1 h after injection) to scan 2 (1–2 h after injection) and scan 3 (3–4 h after injection). (B) Prominent activity is seen in liver, which decreases over time. Focal uptake posteromedially is uptake along adrenal (SUV 5.6). (C) Cardiac activity is most prominent in early images, decreasing with time; distribution is seen along the ventricular myocardium. (D) Diffuse uptake is seen along pancreas (SUV 3.5); posteromedial uptake is physiologic uptake in adrenal gland. (E) Uptake is seen in prostate (SUV 5.6).

patients with neuroblastoma were 0.36 ± 0.26 h for the α phase (57.6%) and 7.3 ± 4.6 h for the β phase (42.4%). Whole-body biologic clearance was monoexponential, with a mean half-life (±SD) of 1.95 ± 1.22 h (range, 1.2–5.2 h) (Fig. 1B).

Biodistribution and Normal-Organ Uptake

^{18}F-MFBG biodistribution (Fig. 2A) was characterized by a rapid drop in the cardiac blood-pool activity (Figs. 2A and 2C). Activity in the urinary bladder was seen early with significant excretion—an average of 45% within the first hour and 61%–95% excretion noted by 3–4 h after injection. Liver showed prominent activity that decreased with time; diffuse uptake in the left lobe of the liver (mean SUV_{max}, 6.0; range, 2.3–11.8) was greater than that in the right lobe (mean SUV_{max}, 3.9; range, 1.1–7.1) (Fig. 2F). The mean biologic liver clearance half-time ($T_{1/2}$) was 80 min. Uptake in the ventricular myocardium (mean SUV_{max}, 3.9; range, 0.63–7.8 at 1 h after injection) showed an initial prominent decrease followed by minimal decrease at later times (Figs. 2A and 2C). Renal activity was mainly in the pelvicalyceal system, with minimal activity seen in the cortex. Diffuse mild splenic activity was seen (mean SUV_{max}, 1.5; range, 0.72–2.7 at 1 h after injection). Salivary gland uptake was prominently seen at all scanning time points, with a decrease in later scans (mean SUV_{max}, 8.6; range, 3.8–12.4 at 1 h after injection). Lacrimal gland activity was seen, also decreasing in later images (mean SUV_{max}, 3.1; range, 0.68–3.8 at 1 h after injection). Prostate gland uptake was seen in males (mean SUV_{max}, 8.6; range, 4.6–10.8 at 1 h after injection). Physiologic uptake was seen in adrenal glands and pancreas with an average SUV_{max} of 6.3 (range, 3.9–9.2) and 3.6 (range, 1.23–5.8), respectively. Diffuse physiologic thyroid uptake was also seen (mean SUV_{max}, 3.5; range, 0.7–6.8 at 1 h after injection). Organ uptake curves are shown in Figure 3.

TABLE 1
^{18}F-MFBG: Normal-Organ Absorbed Doses

	mGy/MBq		cGy/mCi	
Organ	Mean	SD	Mean	SD
Salivary gland	0.058	0.069	0.213	0.253
Adrenals	0.023	0.024	0.085	0.089
Brain	0.004	0.002	0.014	0.008
Breasts	0.005	0.002	0.017	0.008
Gallbladder wall	0.012	0.005	0.046	0.020
Lower large intestine wall	0.011	0.005	0.041	0.020
Small intestine	0.009	0.004	0.033	0.015
Stomach wall	0.007	0.003	0.027	0.012
Upper large intestine wall	0.009	0.004	0.032	0.014
Heart wall	0.031	0.016	0.115	0.057
Kidneys	0.028	0.025	0.105	0.092
Liver	0.046	0.026	0.171	0.097
Lungs	0.009	0.005	0.035	0.017
Muscle	0.006	0.003	0.024	0.010
Ovaries	0.011	0.005	0.041	0.019
Pancreas	0.032	0.021	0.119	0.078
Red marrow	0.006	0.002	0.022	0.008
Osteogenic cells	0.007	0.004	0.027	0.013
Skin	0.004	0.002	0.015	0.007
Spleen	0.015	0.008	0.057	0.028
Testes	0.008	0.006	0.030	0.023
Thymus	0.006	0.003	0.022	0.010
Thyroid	0.032	0.028	0.119	0.103
Urinary bladder wall	0.186	0.195	0.689	0.720
Total body	0.011	0.011	0.042	0.041
Effective dose (mSv/MBq)/ *(cSv or rem/mCi)	0.023	0.012	0.085*	0.043*

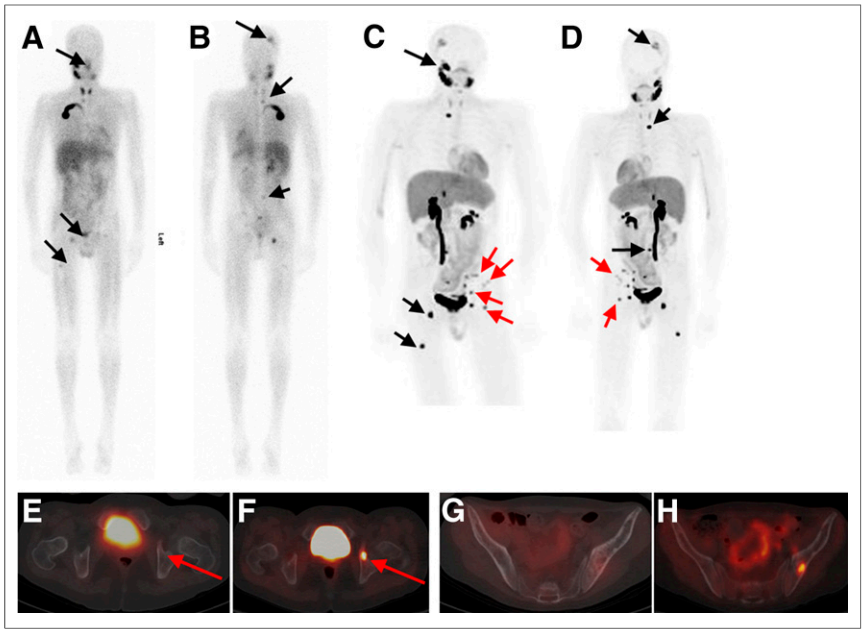

FIGURE 4. Patient with neuroblastoma for follow-up evaluation and possible therapy with ^{131}I-MIBG. ^{123}I-MIBG images (A, anterior; B, posterior) show foci of suspicious activity in skull, lumbar vertebra, right and left acetabula, and right femur (black arrows). Patient underwent imaging with 162 MBq of ^{18}F-MFBG a wk later. Whole-body maximum-intensity-projection scans with ^{18}F-MFBG (C and D) show all lesions seen on ^{123}I-MIBG scan but with greater contrast and clarity (black arrows). In addition, several lesions are seen on ^{18}F-MFBG scan only (red arrows) that are not visible on ^{123}I-MIBG images. For example, fused PET/CT transaxial ^{18}F-MFBG image (F) shows intense uptake in left acetabulum (red arrow), suspicious for disease, that is not seen on ^{123}I-MIBG SPECT/CT fused transaxial image (E). Also, left iliac bone lesions are clearly avid on ^{18}F-MFBG (H) vs. ^{123}I-MIBG imaging (G).

Radiation Doses to Normal Organs

The average absorbed dose estimates are summarized in Table 1. The urinary bladder wall received the highest radiation dose, with a mean absorbed dose (±SD) of 0.186 ± 0.195 mGy/MBq (0 0.689 ± 0.720 cGy/mCi). The mean absorbed dose to salivary glands was 0.058 ± 0.069 mGy/MBq (0.213 ± 0.253 cGy/mCi), liver was 0.046 ± 0.026 mGy/MBq (0.171 ± 0.097cGy/mCi), and kidney was 0.028 ± 0.025 mGy/MBq (0.105 ± 0.092 cGy/mCi). The myocardial/heart wall absorbed dose was 0.031 ± 0.016 mGy/MBq (0.115 ± 0.057 cGy/mCi). The mean total-body dose was 0.011 ± 0.011 mGy/MBq (0.042 ± 0.041 cGy/mCi), and the mean effective dose was 0.023 ± 0.012 mSv/MBq (0.085 ± 0.043 cSv [rem]/mCi).

Preliminary Assessment of Lesion Targeting and Uptake

Targeting of lesions was seen in all patients. Both skeletal and soft-tissue lesions were visualized with high contrast, even in the initial scans acquired 30–60 min after injection, with most lesions seen at 3–4 h after injection. The mean (±SD) lesion SUV_{max} for body weight was 8.6 ± 9.6 (range, 1.3–67.6) at 1–2 h after injection and 9.2 ± 11.4 (range, 1.1–80.7) at 3–4 h after injection. The tumor-to-background (T/BG) ratios obtained by comparison of bone with adjacent normal bone and muscle for soft tissue ranged from 1.35 to 36.2 at 1–2 h after injection and 1.22 to 28.5 at 3–4 h after injection for bone lesions and 1.2 to 35.2 at 1–2 h after injection and 1.4 to 31.4 at 3–4 h after injection for soft-tissue lesions. The lung lesions were visualized at lower uptake because of no uptake in the lungs, with an SUV range of 1.3–4.7 at 1–2 h after injection and 0.8–5.0 at 3–4 h after injection.

Assessment of lesions detected at various imaging times indicated that 103 lesions were seen at 30- to 60-min imaging, and 117 lesions were detected at 1- to 2-h imaging as compared with 122 lesions at 3- to 4-h imaging. The 5 additional lesions seen at the last time point of imaging were seen in the liver of 2 patients (Fig. 4). All lesions seen on ^{123}I-MIBG imaging were seen on ^{18}F-MFBG scans. There were no lesions seen by ^{123}I-MIBG that were not targeted by ^{18}F-MFBG. However, ^{18}F-MFBG showed additional lesions in all patients, with an overall 122 lesions seen versus 63 by ^{123}I-MIBG (Table 2). An additional 59 sites seen on ^{18}F-MFBG included bones (n = 29) and 30 soft-tissue lesions, comprising lung (n = 6), liver (n = 8), nodes (n = 10), and other soft-tissue lesions (n = 6).

DISCUSSION

Given the current limitations of imaging with ^{123}I-MIBG, and in an effort to develop a better imaging biomarker for NETs, we performed first-in-human imaging with ^{18}F-MFBG in 10 patients with metastatic neuroblastoma and paraganglioma/pheochromocytoma. The purpose of this study was to determine the safety, pharmacokinetics, normal-tissue distribution, and organ dosimetry of ^{18}F-MFBG. In addition, an initial evaluation of tumor-targeting properties and detection of lesions at various time points of imaging after injection was performed.

^{18}F-MFBG injections were well tolerated, with no toxicity or reactions seen in any patients. The overall distribution of ^{18}F-MFBG appeared similar to that of ^{123}I-MIBG. The ^{18}F-MFBG distribution showed rapid clearance from the blood pool, with a mean biologic $T_{1/2}$ of 18 min for early phase and 6 h for slower phase. Although prominent uptake was seen in normal liver, the activity decreased with time and lesions were detectable at 1 h after injection with high contrast, though later images showed more contrast and a higher number of lesions in some patients. The differential uptake in the right versus left lobe was noted, as with ^{123}I-MIBG scans. Although the exact mechanism for this difference is unknown, it is postulated to be secondary to differential blood supply and not due to direct uptake mechanism (*20*). The kidneys were the primary route of excretion and the bladder was the critical organ, similar to ^{123}I-MIBG. Because excreted activity accumulates in the bladder by 1 h, voiding before imaging will reduce bladder exposure. With respect to ^{123}I-MIBG biodistribution, similar ^{18}F-MFBG myocardial uptake was seen, and although prominent in the initial scans, the activity decreased with time. Gastrointestinal uptake was seen but was not prominent and did not affect the detection of small lesions in the abdomen and pelvis. Additionally, because of the superior resolution of PET compared with SPECT, it is possible to visualize uptake in lesions in the abdomen and pelvis that would otherwise be obscured by excreted activity in the bowel, ureters, and bladder.

TABLE 2
Lesion Detection Per Patient with ^{18}F-MFBG and ^{123}I-MIBG

Patient no.	^{123}I-MIBG + lesion no.	^{18}F-MFBG + lesion no.
Neuroblastoma		
1	9	11
2	2	3
3	2	5
4	1	2
5	8	13
Pheochromocytoma/ paraganglioma		
1	2	6
2	14	29
3	2	4
4	9	20
5	14	29

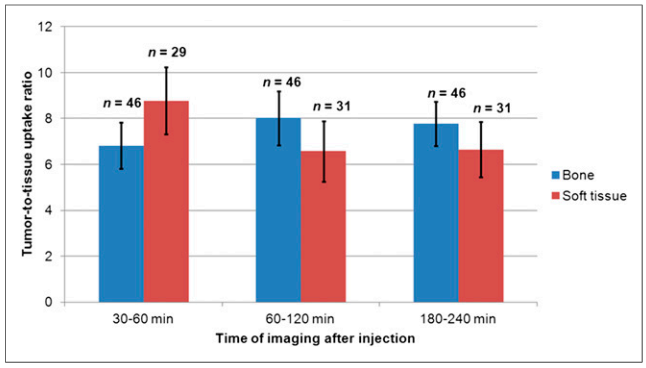

FIGURE 5. Tumor–to–normal bone and soft-tissue uptake ratios at different scan times after injection of ^{18}F-MFBG (scan 1 at 30–60 min, scan 2 at 60–120 min, and scan 3 at 180–240 min). Uptake ratios were based on mean SUVs in respective tissues of 10 patients. Numbers = number of observations (i.e., lesions); error bars = SE of mean.

The clearance of ^{18}F-MFBG from the blood pool and organs is more rapid than ^{123}I-MIBG when compared with published data (*21,22*). As with ^{123}I-MIBG, the blood clearance of ^{18}F-MFBG was biexponential with a shorter biologic $T_{1/2}$ (second component) for ^{18}F-MFBG (ranging between 2 and 15 h) compared with ^{123}I-MIBG (ranging between 9 and 130 h) (*22*). In addition, there was faster and increased excretion into the urine of ^{18}F-MFBG (61%–95%) compared with ^{123}I-MIBG (11%–26%) (*22*) by 3 h after injection. The whole-body biologic $T_{1/2}$ was monoexponential for ^{18}F-MFBG up to 3- to 4-h imaging and was much shorter (1.2–5.2 h) in comparison to the biexponential ^{123}I/^{131}I-MIBG clearance, with a second-phase $T_{1/2}$ of 19–45 h (*21*). The shorter half-time or faster clearance allows for earlier imaging and detection of lesions as a result of high contrast and T/BG ratios noted as early as 1 h after injection, compared with the recommended 24 h postinjection imaging for ^{123}I-MIBG. The radiation exposure (overall effective dose) for ^{18}F-MFBG (0.023 mSv/MBq) was comparable to that of ^{123}I-MIBG (0.014 mSv/MBq for adults and 0.026 mSv/MBq for 10 y olds (*3,21–23*)). The relative organ doses from ^{18}F-MFBG were also comparable to those of ^{123}I-MIBG—lower for liver and spleen and slightly higher for heart with ^{18}F-MFBG. The fact that the effective doses are similar despite faster blood and whole-body clearance is likely secondary to the higher energy associated with the ^{18}F emissions.

The PET images provided high-contrast visualization of lesions due to rapid blood and whole-body background clearance of ^{18}F-MFBG, resulting in high T/BG ratios. ^{18}F-MFBG showed good targeting of both bone and soft-tissue lesions, and high T/BG ratios were noted for both (Fig. 5). Despite modest uptake in the liver, lesions were detectable with relatively high contrast at the 3- to 4-h postinjection imaging times (Figs. 2 and 4). We found that both bone and soft-tissue lesions showed high uptake and were prominently visualized at both 1–2 h and 3–4 h postinjection imaging times, with no statistically significant difference between uptake in lesions at 1–2 h after injection versus 3–4 h after injection ($P = 0.31$ for bone and 0.23 for soft tissue). Given the high contrast of ^{18}F-MFBG images, it is possible to image patients with lower activities, which can further reduce radiation exposure (images in Figs. 4C and 4D were obtained with a 162 MBq dose of ^{18}F-MFBG).

Although tracer uptake in lesions continued to increase up to the last imaging time point (3–4 h after injection), a decrease in the T/BG ratios was noted at 3–4 h after injection. Although the overall number of lesions detected was highest for the last time point of imaging, no statistically significant difference was evident in the number of lesions detected between 1 and 2 h after injection versus 3 and 4 h after injection ($P = 0.24$). Five additional lesions were detected at 3–4 h postinjection imaging versus 1- to 2-h imaging and were liver lesions seen in 2 patients. However, other liver lesions present in these 2 patients were detected at both 1- to 2-h and 3- to 4-h imaging. Given that imaging at 1–2 h after injection showed the highest T/BG ratios for both soft-tissue and bone lesions, this would be the optimal time point for imaging to provide adequate high-contrast images and good lesion detection (Fig. 3).

^{123}I-MIBG is Food and Drug Administration–approved for imaging neuroendocrine malignancies and is extensively used in the clinical assessment of neuroblastoma (*24*). The biodistribution of ^{18}F-MFBG is similar to that of ^{123}I-MIBG, with the added advantage of clearing more rapidly from the body as well as higher resolution and improved assessment of lesion uptake (SUV) by PET imaging. Another advantage of ^{18}F-MFBG, particularly in pediatric patients, is the ability to image with PET/MR, which would reduce radiation exposure by eliminating the CT component of imaging. ^{18}F-MFBG PET/CT imaging also overcomes several limitations of ^{123}I-MIBG SPECT/CT imaging, such as offering single-day imaging at 1–2 h after injection versus a 2-d imaging procedure as well as reducing the lag time for scanning after injection, thereby providing a more convenient option for patients.

CONCLUSION

Imaging with ^{18}F-MFBG is feasible and safe. It is well tolerated by adults and pediatric patients. ^{18}F-MFBG has favorable biodistribution and acceptable organ dosimetry and targets both bone and soft-tissue lesions with high contrast, enabling early imaging at 1–2 h after injection. ^{18}F-MFBG is highly promising for imaging patients with NETs, especially children with neuroblastoma.

DISCLOSURE

This study was funded by the Department of Radiology seed grant of Memorial Sloan Kettering Cancer Center; NIH grant R01 CA204093 (Principal Investigator: Neeta Pandit-Taskar); and the MSK Radiochemistry & Molecular Imaging Probes Core, supported in part by NIH/NCI Cancer Center support grant P30 CA008748. The development of ALP-MFBG–based radiosynthesis was funded in part by a grant from The Hartwell Foundation (Principal Investigator: Scott E. Snyder) and by NIH Research Project grant R01 (NIBIB 5 R01EB015536) (Principal Investigator: Stephen DiMango). No other potential conflict of interest relevant to this article was reported.

REFERENCES

1. Monclair T, Brodeur GM, Ambros PF, et al. The International Neuroblastoma Risk Group (INRG) staging system: an INRG Task Force report. *J Clin Oncol.* 2009;27:298–303.
2. Decarolis B, Schneider C, Hero B, et al. Iodine-123 metaiodobenzylguanidine scintigraphy scoring allows prediction of outcome in patients with stage 4 neuroblastoma: results of the Cologne interscore comparison study. *J Clin Oncol.* 2013;31:944–951.
3. Bombardieri E, Giammarile F, Aktolun C, et al. ^{131}I/^{123}I-metaiodobenzylguanidine (mIBG) scintigraphy: procedure guidelines for tumour imaging. *Eur J Nucl Med Mol Imaging.* 2010;37:2436–2446.
4. Boubaker A, Bischof Delaloye A. MIBG scintigraphy for the diagnosis and follow-up of children with neuroblastoma. *Q J Nucl Med Mol Imaging.* 2008;52: 388–402.
5. Katzenstein HM, Cohn SL, Shore RM, et al. Scintigraphic response by ^{123}I-metaiodobenzylguanidine scan correlates with event-free survival in high-risk neuroblastoma. *J Clin Oncol.* 2004;22:3909–3915.
6. Kushner BH, Yeh SD, Kramer K, Larson SM, Cheung NK. Impact of metaiodobenzylguanidine scintigraphy on assessing response of high-risk neuroblastoma to dose-intensive induction chemotherapy. *J Clin Oncol.* 2003;21:1082–1086.
7. Boubaker A, Bischof Delaloye A. Nuclear medicine procedures and neuroblastoma in childhood: their value in the diagnosis, staging and assessment of response to therapy. *Q J Nucl Med.* 2003;47:31–40.
8. Sisson JC, Shulkin BL. Nuclear medicine imaging of pheochromocytoma and neuroblastoma. *Q J Nucl Med.* 1999;43:217–223.
9. Hartung-Knemeyer V, Rosenbaum-Krumme S, Buchbender C, et al. Malignant pheochromocytoma imaging with [^{124}I]MIBG PET/MR. *J Clin Endocrinol Metab.* 2012;97:3833–3834.
10. Pentlow KS, Graham MC, Lambrecht RM, et al. Quantitative imaging of iodine-124 with PET. *J Nucl Med.* 1996;37:1557–1562.
11. Timmers HJ, Chen CC, Carrasquillo JA, et al. Comparison of ^{18}F-fluoro-L-DOPA, ^{18}F-fluoro-deoxyglucose, and ^{18}F-fluorodopamine PET and ^{123}I-MIBG scintigraphy in the localization of pheochromocytoma and paraganglioma. *J Clin Endocrinol Metab.* 2009;94:4757–4767.
12. Piccardo A, Lopci E, Foppiani L, Morana G, Conte M. ^{18}F-DOPA PET/CT for assessment of response to induction chemotherapy in a child with high-risk neuroblastoma. *Pediatr Radiol.* 2014;44:355–361.
13. Bonfiglioli R, Nanni C, Martignani C, et al. ^{11}C-mHED for PET/CT: principles of synthesis, methodology and first clinical applications. *Curr Radiopharm.* 2014;7:79–83.
14. Garg PK, Garg S, Zalutsky MR. Synthesis and preliminary evaluation of para- and meta-[^{18}F]fluorobenzylguanidine. *Nucl Med Biol.* 1994;21:97–103.
15. Zhang H, Huang R, Cheung NK, et al. Imaging the norepinephrine transporter in neuroblastoma: a comparison of [^{18}F]-MFBG and ^{123}I-MIBG. *Clin Cancer Res.* 2014;20:2182–2191.
16. Zhang H, Huang R, Pillarsetty N, et al. Synthesis and evaluation of ^{18}F-labeled benzylguanidine analogs for targeting the human norepinephrine transporter. *Eur J Nucl Med Mol Imaging.* 2014;41:322–332.
17. Hu B, Vavere AL, Neumann KD, Shulkin BL, DiMagno SG, Snyder SE. A practical, automated synthesis of meta-[^{18}F]fluorobenzylguanidine for clinical use. *ACS Chem Neurosci.* 2015;6:1870–1879.
18. Barrett PH, Bell BM, Cobelli C, et al. SAAM II: Simulation, Analysis, and Modeling Software for tracer and pharmacokinetic studies. *Metabolism.* 1998;47:484–492.
19. Stabin MG, Sparks RB, Crowe E. OLINDA/EXM: the second-generation personal computer software for internal dose assessment in nuclear medicine. *J Nucl Med.* 2005;46:1023–1027.
20. Jacobsson H, Johansson L, Kimiaei S, Larsson SA. Concentration of ^{123}I-metaiodobenzylguanidine in left and right liver lobes: findings indicate regional differences in function in the normal liver. *Acta Radiol.* 1999; 40:224–228.
21. Wafelman AR, Hoefnagel CA, Maes RA, Beijnen JH. Radioiodinated metaiodobenzylguanidine: a review of its biodistribution and pharmacokinetics, drug interactions, cytotoxicity and dosimetry. *Eur J Nucl Med.* 1994;21: 545–559.
22. Lashford LS, Moyes J, Ott R, et al. The biodistribution and pharmacokinetics of meta-iodobenzylguanidine in childhood neuroblastoma. *Eur J Nucl Med.* 1988;13: 574–577.
23. Adreview. Highlights of prescribing information. Food and Drug Administration website. http://www.accessdata.fda.gov/drugsatfda_docs/label/2008/22290lbl.pdf. Accessed October 26, 2017.
24. Brisse HJ, McCarville MB, Granata C, et al. Guidelines for imaging and staging of neuroblastic tumors: consensus report from the International Neuroblastoma Risk Group Project. *Radiology.* 2011;261:243–257.